

Multimodal Dynamic Brain Connectivity Analysis Based on Graph Signal Processing for Former Athletes With History of Multiple Concussions

Saurabh Sihag¹, Sebastien Naze, Foad Taghdiri, Charles Tator, Richard Wennberg, David Mikulis, Robin Green, Brenda Colella, Maria Carmela Tartaglia, and James R. Kozloski

Abstract—The study of structure-function relationships in the brain has been an active area of research in neuroscience. The availability of brain imaging data that captures the structural connectivity and functional co-activation of the brain regions has led to the study of multimodal technical frameworks that can help disentangle the mechanisms linking cognitive abilities and brain structural alterations. This paper analyzes the diffusion and resting state functional magnetic resonance imaging (dMRI and rs-fMRI) data collected from a population consisting of former athletes with

a history of multiple concussions and healthy controls with no reported history of concussion. For each subject, the structural connectome is represented by a graph with its nodes associated with cortical brain regions and the adjacency matrix derived from dMRI. Each cortical brain region is associated with a blood oxygen level dependent (BOLD) signal derived from fMRI. This paper uses the tools from graph signal processing (GSP) to select the brain regions of interest (ROIs) that have significant statistical differences in the extracted high and low graph frequency components of the region specific BOLD signal across former athletes and healthy controls, where the graph frequencies represent the extent of spatial variations of the BOLD signal across the brain. The selected ROIs have also been previously identified to be affected in the existing clinical studies on traumatic brain injuries (TBI). Furthermore, the dynamic functional connectivity profiles of the selected ROIs are determined by leveraging the high and low graph frequency components of the BOLD signal and a sliding window based approach. Interestingly, the graph frequency functional connectivity profiles reveal unique characteristics that are not apparent in the unimodal dynamic functional connectivity profiles based on fMRI. Our analysis reveals statistically significant differences in the dwell times in multiple dynamic graph frequency functional connectivity states for the two groups of subjects. Therefore, the results presented in this paper underline the significance of graph signal processing tools for multimodal analysis of brain imaging data and also provide promising direction for applications in clinical research and medical diagnosis.

Manuscript received July 1, 2019; revised November 26, 2019 and February 29, 2020; accepted March 14, 2020. Date of publication March 23, 2020; date of current version April 20, 2020. The associate editor coordinating the review of this manuscript and approving it for publication was Dr. Antonio Ortega. (Corresponding author: Saurabh Sihag.)

Saurabh Sihag, Sebastien Naze, and James R. Kozloski are with the Computational Biology Center, T.J. Watson IBM Research Center, Ossining, NY 10562 USA (e-mail: sihags@rpi.edu; naze@us.ibm.com; kozloski@us.ibm.com).

Foad Taghdiri is with the Tanz Centre for Research in Neurodegenerative Diseases, University of Toronto, Toronto, ON M5S, Canada (e-mail: foad.taghdiri@mail.utoronto.ca).

Charles Tator is with the Canadian Concussion Center, Toronto Western Hospital, Neuroscience Centre, University Health Network, Toronto, ON M5G 2C4, Canada, with the Institute of Medical Science, University of Toronto, Toronto, ON M5S, Canada, and also with the Division of Neurosurgery, Toronto Western Hospital, Krembil Brain Institute, University Health Network, Toronto, ON M5G 2C4, Canada (e-mail: charles.tator@uhn.ca).

Richard Wennberg is with the Canadian Concussion Center, Toronto Western Hospital, Neuroscience Centre, University Health Network, Toronto, ON M5G 2C4, Canada, and also with the Division of Neurology, Toronto Western Hospital, University Health Network, Toronto, ON M5G 2C4, Canada (e-mail: r.wennberg@utoronto.ca).

David Mikulis is with the Canadian Concussion Center, Toronto Western Hospital, Neuroscience Centre, University Health Network, Toronto, ON M5G 2C4, Canada, with the Institute of Medical Science, University of Toronto, Toronto, ON M5S, Canada, and also with the Division of Neuroradiology, Joint Department of Medical Imaging, University Health Network, Toronto, ON M5G 2C4, Canada (e-mail: david.mikulis@uhn.ca).

Robin Green is with the Canadian Concussion Center, Toronto Western Hospital, Neuroscience Centre, University Health Network, Toronto, ON M5G 2C4, Canada, with the Institute of Medical Science, University of Toronto, Toronto, ON M5S, Canada, and also with the Department of Rehabilitation Sciences, University of Toronto, Toronto, ON M5S, Canada (e-mail: robin.green@uhn.ca).

Brenda Colella is with the Canadian Concussion Center, Toronto Western Hospital, Neuroscience Centre, University Health Network, Toronto, ON M5G 2C4, Canada, and also with the Department of Rehabilitation Sciences, University of Toronto, Toronto, ON M5S, Canada (e-mail: brenda.colella@uhn.ca).

Maria Carmela Tartaglia is with the Tanz Centre for Research in Neurodegenerative Diseases, University of Toronto, Toronto, ON M5S, Canada, and also with the Canadian Concussion Center, Toronto Western Hospital, Neuroscience Centre, University Health Network, Toronto, ON M5G 2C4, Canada (e-mail: carmela.tartaglia@uhn.ca).

This article has supplementary downloadable material available at <http://ieeexplore.ieee.org>, provided by the authors.

Digital Object Identifier 10.1109/TSIPN.2020.2982765

Index Terms—Brain modeling, graphical models, signal processing.

I. INTRODUCTION

A. Literature Review

GRAPHICAL models and complex networks are among the widely adopted tools for mathematical representation and analysis of anatomical structure and functional activation of the brain derived from brain imaging [1]–[3]. In an anatomy based graph model for the brain, the brain regions form the nodes while the number of axonal connections and degree of co-activation between any two brain regions determine the structural connectivity and functional connectivity, respectively, between them.

Existing studies have expanded the analysis of functional connectivity from a static perspective, i.e., studying the average functional coupling among the brain regions across a scan length, to a dynamic perspective, where the focus is on the dynamic evolution of functional connectivity during an entire brain imaging scan [4]–[6]. The evolution of resting state

functional connectivity based on the analysis of functional magnetic resonance imaging (fMRI) data was explored in [7]–[9]. The studies in [9]–[17] focused on evaluating different technical frameworks for dynamic functional connectivity analysis. Specifically, a least squares approach was adopted in [9] to jointly learn the time invariant and time varying connectivity patterns in the functional connectivity. A time varying graphical Lasso based approach was applied in [10] to analyze resting state fMRI. In [11], the dynamic functional connectivity was characterized by a time varying tensor based decomposition of the electroencephalography (EEG) data. A hidden Markov model based Bayesian framework was studied to analyze time varying functional networks and their corresponding change points in [12]. In [13], the instantaneous phase synchrony analysis based approach was investigated for dynamic connectivity analysis of fMRI. The study in [14] adopted a data driven principal component analysis (PCA) based methodology to analyze time varying patterns in the fMRI data. The study in [15] analyzed the dynamic functional connectivity for an anatomical graph model and a data driven independent component analysis (ICA) based graph model of the brain. In [16], the correlation between the results from dynamic connectivity analysis of the fMRI data and features extracted from EEG data was investigated.

The study of dynamic functional connectivity has also been applied in clinical studies to isolate the functional changes in the brain in the context of various neurodegenerative diseases and neuropsychiatric disorders [18]–[30]. Specifically, the time varying functional connectivity derived from the fMRI data analysis has been investigated in the studies on Alzheimer's disease [18], schizophrenia [19]–[21], psychosis [22], epilepsy [23], behavioral weight loss [25], Parkinson's disease [26], depression [27], and mild traumatic brain injury (mTBI) [28]–[30]. The studies in [28]–[30] analyzed the dynamic functional connectivity for subjects with mTBI using resting state functional magnetic resonance imaging (fMRI) data. In [28], different intrinsic connectivity networks were identified from the blood oxygen level dependent (BOLD) signal using independent component analysis and their functional connectivity analyzed using a sliding window approach. The study in [29] reported the effects of fMRI data preprocessing routines on the results of the dynamic functional connectivity analysis for mild traumatic brain injury. In [30], the dynamic functional connectivity was analyzed for subjects at the acute stage of mTBI and those diagnosed with post-concussive syndrome (PCS).

The alterations in the structural and functional connectivity of the brain due to traumatic brain injuries have been studied using the tools from graph theory and network analysis in [31]–[38]. Changes in structural integrity and functional connectivity of the brain were analyzed independently and correlated in [31]. A graph theory based approach to analyze the alterations in functional connectivity due to TBI was proposed in [32]. The evolution of disruptions in functional connectivity over a period of time were studied for subjects diagnosed with PCS [36]. The variations in structural connectivity due to brain injury were studied and correlated with cognitive flexibility in [37]. In [38], features from resting state fMRI and diffusion MRI were evaluated for detection of TBI using a machine learning framework.

The aforementioned studies in [28]–[38] in the context of brain imaging data analysis for TBI, analyzed the functional and structural connectivity independently. The availability of brain imaging techniques that capture the brain structural connectivity (e.g., diffusion magnetic resonance imaging (dMRI)) and functional connectivity (e.g., EEG, fMRI) have allowed the multimodal analysis based on anatomical and functional connectivity of the human brain and therefore, a better comprehension of the neuropsychological significance of the features extracted from brain imaging data [39]. Multimodal brain imaging analysis is particularly relevant in the context of traumatic brain injuries (TBI), where the anatomical and functional alterations in the brain have been reported to be correlated with behavioral and cognitive dysfunctions [40]–[43]. Alterations in the functional behavior of default mode network during visual tasks for subjects with mTBI was studied in [40]. The structural connectivity of the brain was correlated with neurocognitive functioning for subjects at different stages of recovery from TBI [41]. Features in functional connectivity for subjects with TBI were reported to be correlated with performance in switching tasks and severity of injury in [42].

Multimodal analyses of brain imaging data have been applied to relate the structure-function relationships with cognitive impairment and flexibility in different contexts besides TBI in [39], [44]–[57]. A review of ICA based multimodal fusion techniques and their role in the study of psychopathology was provided in [39]. In [44], the structural alterations in white matter and gray matter were studied in the context of autism spectrum disorder. Supervised learning algorithms on structural and functional connectivity data were shown to be effective for age prediction in [45]. The study in [46] analyzed the relationships between the resting state networks and spectral properties of the human brain connectome.

The domain of graph signal processing (GSP), which enables the analysis of signals generated on the nodes of a graph, has provided a promising framework for multimodal analyses of brain imaging data. In recent years, GSP analysis has been applied to the joint analysis of the human brain structural and functional networks in [48]–[57]. The studies in [48]–[50] related the performance and adaptability over different tasks with the energies of the graph frequency components of the blood oxygen-level dependent (BOLD) signal associated with brain activity. In [51], dimensionality reduction and supervised learning strategies were applied in conjunction with graph signal processing tools to evaluate the classification performance on datasets of brain signals collected under different contexts. The study in [52] focuses on analyzing the coupling between function and structure for different brain regions using graph filtering operations.

Limited studies have explored the use of GSP frameworks for finding discriminating features in different contexts of neurological disorders [53]–[57]. A low graph frequency based classification framework was studied in the context of Alzheimer's disease in [53]. The studies in [54], [55] studied the MRI brain imaging data in the context of autism spectrum disorder (ASD) and focused on finding the features derived from graph signal processing for supervised classification tasks. Specifically, the study in [54] used time varying coefficients of graph Fourier

transform for supervised classification. The works in [56] and [57] used graph signal processing tools on electroencephalography (EEG) data in the context of consciousness disorders and schizophrenia, respectively.

B. Contributions

In this paper, we used the tools from graph signal processing to analyze the dynamic functional connectivity of the brain in the context of concussion. The brain imaging data (dMRI and fMRI) were collected from two groups of subjects: 55 former athletes with a history of multiple concussions and 26 healthy controls with no reported history of concussions. Graph filters based on the spectral decomposition of the structural connectivity of the brain were used to extract the different components of the BOLD signals according to their spatial variability over the brain structure. We used the energies of the high graph frequency and low graph frequency components of the subjects' BOLD signals as features to select the regions of interest in the brain that had statistically significant variations in the two groups of subjects. Based on the high graph frequency analysis, we selected 5 regions of interest (ROIs): entorhinal, isthmus cingulate, superior parietal, precuneus, and insula in the left hemisphere, and analyzed the dynamic high graph frequency functional connectivity of these regions. Similarly, based on the low graph frequency analysis, we selected 8 regions of interest: supramarginal, para hippocampal, postcentral, and superior parietal in the left hemisphere and pericalcarine, pars opercularis, pars triangularis, and postcentral in the right hemisphere, and analyzed the dynamic low graph frequency functional connectivity of these regions. The analysis of time varying connectivity of the regions of interest, where the connectivity between any two regions was determined by the correlation among their respective graph filtered components of the BOLD signal, established a multimodal dynamic functional connectivity analysis framework. Dynamic graph frequency based functional connectivity analysis pertaining to low graph frequency and high graph frequency components of the BOLD signal in the respective ROIs revealed statistically significant variations in the dynamic connectivity profiles in different graph frequencies for former athletes and healthy controls.

II. DATA ACQUISITION

The study was approved by the research ethics boards of University Health Network. Consent was obtained from all subjects before participating in the study. The 55 former athletes (mean age = 51.61 years, standard deviation = 12.74 years) were male former professional football, hockey or boxing athletes, with history of multiple concussions and thus at risk of a neurodegenerative disease such as chronic traumatic encephalopathy (CTE). Healthy subjects (number = 26, mean age = 50.20 years, standard deviation = 12.14 years) were recruited from the community and were healthy male volunteers with no history of concussion.

High-resolution T1-weighted whole-brain scans were acquired using inversion recovery fast spoiled gradient echo (IR-FSPGR) sequence and the following parameters: 180 axial slices with 1 mm thickness; 3-ms echo time (TE); 7.8-ms

repetition time (TR); 450-ms inversion time (TI); 15 flip angle; 25.6-cm field of view (FOV); 256×256 matrix size; $1 \times 1 \times 1$ mm³ voxel size. A 3 T MRI system (Signa HDx, GE Healthcare, Milwaukee, WI, USA) with a standard 8-channel head coil was used to obtain structural and diffusion-weighted imaging (DWI) and the following parameters: 2.4 mm thick axial slices, TR = 17000 ms, FOV = 23 cm, 2.4×2.4 mm² in-plane resolution. At least one DWI scan was obtained per subject with diffusion gradients applied across 60 spatial directions ($b=1000$ s/mm²) as well as 10 non-diffusion weighted (B0) scans. Prior to the rs-fMRI scan, participants were instructed to close their eyes, not think of anything in particular, and to not fall asleep. The scan acquisition was 5 min 8 s using T2-weighted echo-planar imaging with the following parameters: TR = 2000 ms, TE = 30 ms, 64×64 matrix, 20-cm FOV, flip angle = 85°, 40 slices, $3.125 \times 3.125 \times 4$ mm³ voxels.

III. METHODS

We first list the standard methodologies utilized to extract the structural and functional connectivity data for each subject.

A. Multi-Modal Neuroimaging Pipeline

We utilized the MRI/dMRI pipeline from [58] to extract the subject specific structural connectomes from dMRI data. The structural connectome for each subject was formed by 66 cortical brain regions. The pipeline was based on FreeSurfer, FSL, and the MRtrix3 tractography toolbox and computed a 66×66 cortico-cortical connectivity matrix that conformed to the Desikan-Kiliany brain parcellation (*Unknown* and *Corpus Callosum* regions were not considered cortical, and therefore we removed them bilaterally from our study) and was subsequently normalized by regions' volume. Note that Corpus Callosum was only removed as a node and the inter-hemispheric fibres passing through Corpus Callosum were represented as edges and accounted for in the structural connectivity matrix computed by the MRI/dMRI pipeline.

The blood oxygen level dependent (BOLD) time series from fMRI data was extracted using the fMRIPrep pipeline [59]. The region wise BOLD time series were extracted by region-based averaging of the time series using the Desikan-Kiliany cortical parcellation. The extracted BOLD time series were of length 308 seconds (154 time points) of which the first 18 seconds were not utilized in the analysis in this paper. Additionally, the BOLD time series were pre-processed by removal of any linear trends and constant offsets and passed through a second order Butterworth low pass frequency domain filter with the cutoff frequency 0.1 Hz. To account for any variations in the fMRI data across the subjects due to physical aspects of MRI scanning, the BOLD time series per region were z-score normalized [60].

B. ROI Selection Using Graph Signal Processing Analysis

We briefly discuss the theory of graph Fourier transform (GFT) and graph filters used for feature extraction and ROI selection from the brain imaging data.

1) *Brain Graph Model*: The structural connectome of a subject's brain is represented in the form of a cortico-cortical structural connectivity matrix derived from its MRI/dMRI data, and presents one input to our pipeline. Consider a brain structural connectivity graph $\mathcal{G} \triangleq \{\mathcal{V}, \mathcal{E}\}$, where \mathcal{V} is the set of nodes with each node representing a distinct cortical brain region, s.t., $|\mathcal{V}| = n$, and \mathcal{E} is the set of undirected edges in \mathcal{G} . The edge between a pair of distinct regions i and j , if it exists, is denoted by (i, j) . Therefore, the cortico-cortical structural connectivity matrix describes the adjacency matrix of the brain structural connectivity graph. Define $\mathbf{A} \in \mathbb{R}^{n \times n}$ as the weighted adjacency matrix, s.t.,

$$A_{ij} = \begin{cases} w_{ij}, & \text{if } (i, j) \in \mathcal{E}, \\ 0, & \text{if } (i, j) \notin \mathcal{E} \text{ or if } i = j. \end{cases} \quad (1)$$

where A_{ij} is the entry in \mathbf{A} that represents the axonal tract link between i -th and j -th cortical region in the brain, $\forall i \neq j \in \mathcal{V}$ and $w_{i,j} > 0$ is the strength of the link A_{ij} . Each node is associated with a collection of measurements, which in this paper, is the BOLD time series extracted from fMRI data. Define $\mathbf{X} \in \mathbb{R}^{n \times t}$ as the BOLD signal for n brain regions over the course of t time points.

2) *Graph Frequency Analysis*: The graph frequencies correspond to the specific components of the BOLD signal according to the degree of their variability on the physical structure of the brain [48]. Graph Fourier Transform (GFT) [61] provides the necessary framework to encode this variability of BOLD time series over structural connectome into graph frequencies. We define GFT as follows:

Definition 1 (Graph Fourier Transform): Given a signal $x \in \mathbb{R}^n$ and a diagonalizable graph shift operator $\mathbf{S} = \mathbf{V}\mathbf{\Lambda}\mathbf{V}^{-1} \in \mathbb{R}^{n \times n}$, the graph Fourier transform pair is given by

$$\hat{x} = \mathbf{V}^{-1}x, \quad \text{and} \quad x = \mathbf{V}\hat{x}. \quad (2)$$

In general, the adjacency matrix and the variants of the Laplacian matrix can be used as graph shift operators [48]. In this paper, we use the adjacency matrix \mathbf{A} as the graph shift operator. Since \mathbf{A} is a symmetric matrix, we have $\mathbf{V}^{-1} = \mathbf{V}^T$. The eigenvectors of $\mathbf{A} = \mathbf{V}\mathbf{\Lambda}\mathbf{V}^{-1}$ form the columns of $\mathbf{V} = [v_0, \dots, v_{n-1}]$. The eigenvalues of \mathbf{A} are the elements of the diagonal matrix $\mathbf{\Lambda} = \text{diag}(\lambda_0, \lambda_1, \dots, \lambda_{n-1})$. Note that the eigenvectors of \mathbf{A} form the spectral components of the graph and the eigenvalues of \mathbf{A} form the graph frequencies. The eigenvector-eigenvalue pairs, $(v_k, \lambda_k), \forall k \in \{0, \dots, n-1\}$, of \mathbf{A} are termed as the eigenmodes of the graph \mathcal{G} .

In GSP, the graph frequencies are associated with the spatial variation of the signal across the graph. This can be intuitively explained by the relation of the graph frequencies with the total variation of the spectral components given by

$$\text{TV}_G(v_k, \lambda_k) \triangleq \|1 - \lambda_k / \lambda_{\max}(\mathbf{A})\|_1 \|v_k\|_1, \quad (3)$$

where $\lambda_{\max}(\mathbf{A})$ is the largest eigenvalue of \mathbf{A} and $\|\cdot\|_1$ is the ℓ_1 norm. Based on (3), the graph frequency λ_l is said to be higher than λ_k if $\text{TV}_G(v_l, \lambda_l) > \text{TV}_G(v_k, \lambda_k)$ [61]. Note that for

adjacent matrix \mathbf{A} , we have

$$\lambda_k = v_k^T \mathbf{A} v_k = \sum_{i \neq j} A_{ij} v_k^i v_k^j, \quad (4)$$

where v_k^i is the i -th element of the eigenvector v_k . Thus, a large value of λ_k implies smaller variation in the elements associated with connected nodes in the eigenvector corresponding to λ_k , whereas, the smaller eigenvalues imply that the entries of their corresponding eigenvectors at the structurally connected nodes tend to be in different directions. For the GSP analysis with the adjacency matrix as the graph shift operator, the *lower graph frequencies are associated with the larger eigenvalues*.

3) *Graph Spectral Filtering*: The theory behind graph frequencies summarized in Section III-B2 allows us to extract different components of the BOLD time series according to their spatial variation with the help of graph frequency filters [62], which act as the second input to our pipeline. We define a graph filter

$$\mathbf{F} \triangleq \text{diag}(f(\lambda_0), \dots, f(\lambda_{n-1})), \quad (5)$$

where $f(\lambda_k)$ is the frequency response for the eigenmode $k \in \{0, \dots, n-1\}$. For a given spatial vector x over the graph, its graph filtered output y is given by

$$y = \mathbf{V}\mathbf{F}\mathbf{V}^T x. \quad (6)$$

As an example, a high pass graph filter that passes only the components corresponding to 10 highest graph frequencies can be designed by setting the diagonal elements

$$f(\lambda_k) = \begin{cases} 1, & \forall k = \{0, \dots, 9\} \\ 0, & \text{otherwise.} \end{cases} \quad (7)$$

The design of the graph filters enabled us to isolate the different frequency components of BOLD signals for the subjects. For this purpose, we first used the GFT based filter to extract the graph frequency components of the BOLD time series $\mathbf{X} \in \mathbb{R}^{n \times t}$, which is given by

$$\mathbf{Y} = \mathbf{V}\mathbf{F}\mathbf{V}^T \mathbf{X}, \quad (8)$$

where $\mathbf{Y} \in \mathbb{R}^{n \times t}$ is the graph frequency component of \mathbf{X} corresponding to the graph filter \mathbf{F} . To evaluate the energy of the graph frequency component of \mathbf{Y} at a brain region $i \in \mathcal{V}$, we evaluated the ℓ_2 norm of \mathbf{Y}_i where \mathbf{Y}_i is the i -th row of \mathbf{Y} , s.t., $\mathbf{Y} = [\mathbf{Y}_1, \dots, \mathbf{Y}_n]^T$.

We focused our analysis on the high graph frequency and low graph frequency components of the BOLD signal that have been consistently shown to be the most informative and robust for brain imaging analysis [49], [50]. The eigenvalues for the two groups of subjects were not different significantly. Fig. 1 illustrates the eigenspectrum of the structural connectome for different subjects. For every subject, we used the 7 highest eigenvalues for low pass graph filtering and 6 lowest eigenvalues for the high pass graph filtering. The robustness of the decomposition of the BOLD signals with respect to the cutoffs on the graph frequencies for graph filtering was verified using similar methods adopted in [49] and [50]. See supplementary file for more details.

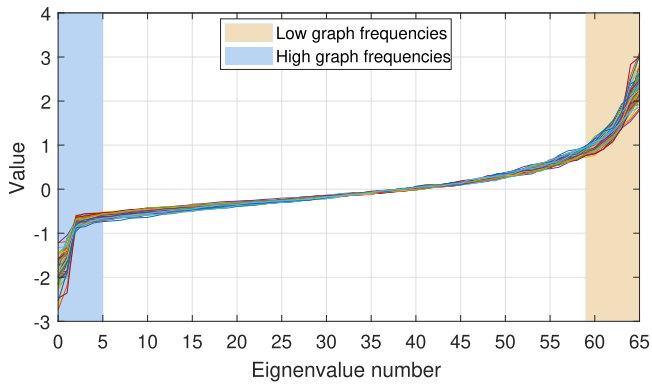


Fig. 1. Eigenspectra of the adjacency matrices of the structural connectomes of all 81 subjects. For each subject, the lowest eigenvalues (in blue background) were associated with the high graph frequencies and the highest eigenvalues (in yellow background) were associated with the low graph frequencies.

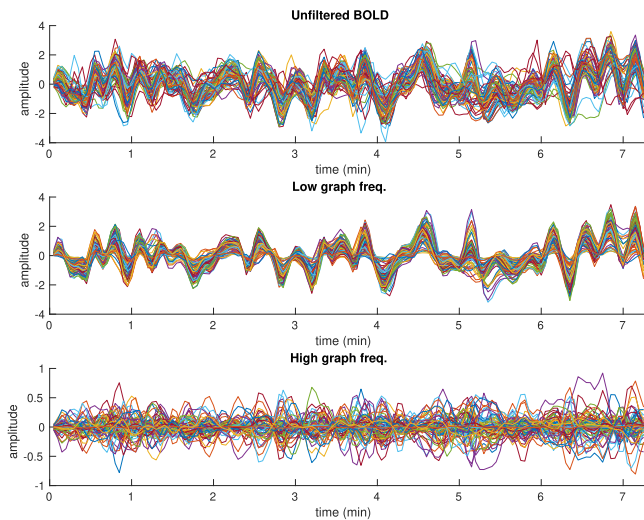


Fig. 2. BOLD time series from the 66 parcellated cortical brain regions of a randomly selected subject, with corresponding low and high graph frequencies filtered BOLD signals. For all 66 brain regions, note the smooth spatial evolution in the low pass filtered BOLD time series and highly variable spatial evolution in the high pass filtered BOLD time series.

Fig. 2 shows the high graph frequency components and low graph frequency components of the BOLD signal from all 66 brain regions for a randomly selected subject. The output of the low pass graph filter varies smoothly for all brain regions. On the other hand, the output of the high pass graph filter exhibits rapid variation across different brain regions which illustrates high spatial variability. The magnitudes of the unfiltered BOLD signals capture the neuronal activities at different brain regions.

Figs. 3 and 4 plot the mean energies (ℓ_2 -norms) of the high graph frequency components and the low graph frequency components for different brain regions, respectively, for the two groups of subjects. The brain regions are grouped by coarser anatomical affinity (frontal, temporal, occipital, parietal, and insular lobes). As expected, the low pass graph filters capture more energy as compared to the high pass graph filters because the BOLD signals at different inter-connected brain regions tend to change in the same direction. The brain functional activity that

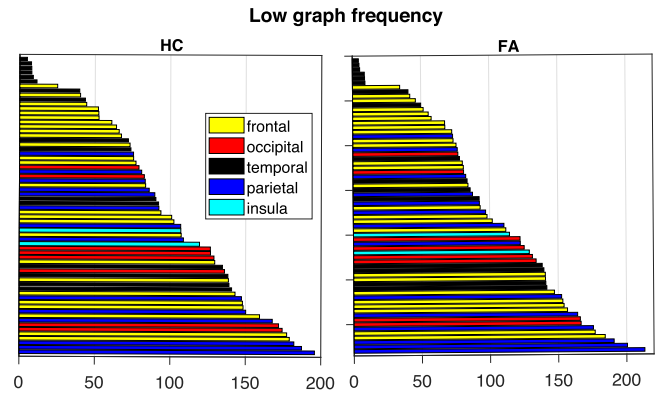


Fig. 3. Energy concentrations of low graph frequency components sorted from lowest to highest across all areas for healthy subjects (HC) and former athletes (FA). The bars represent the mean energy concentration of the low graph frequency components in 66 brain areas across the two groups of subjects and are color-coded by the lobe assignment.

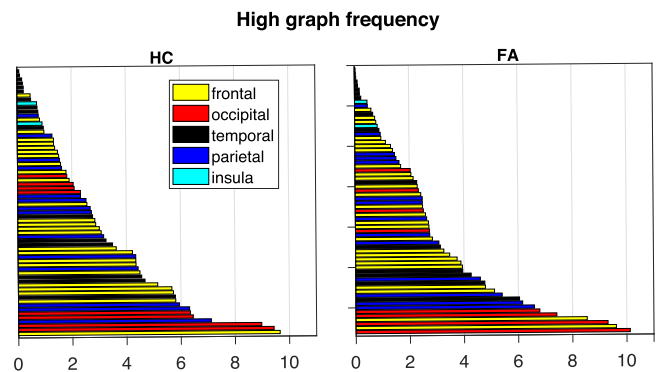


Fig. 4. Energy concentrations of high graph frequency components sorted from lowest to highest across all areas for healthy subjects (HC) and former athletes (FA). The bars represent the mean energy concentration of the high graph frequency components in 66 brain areas across the two groups of subjects and are color-coded by the lobe assignment.

deviates from this trend is captured by the high pass graph filters. Furthermore, for both healthy subjects and former athletes, we observed that the low graph frequency components had higher energies for the brain regions in the parietal lobe and the occipital lobe (see Fig. 2 in the supplementary file). Also, the high graph frequency components were more concentrated in the certain regions of the occipital lobe (see Fig. 1 in the supplementary file). However, there were subtle differences between the distributions of the energies of high or low graph frequency components across the different lobes in the former athletes and healthy controls. To isolate the significant differences between the two groups, energies of the different graph frequency components of the BOLD signals from the 66 brain regions were statistically compared for the two groups of subjects.

The corresponding variances of the energy concentrations of the low graph frequency components in Fig. 3 or that of the high graph frequency components in Fig. 4 across subjects were assessed individually for every brain region using an F-test at 0.05 significance level with the null hypothesis that the variances of the distributions of the low or high graph frequency energy

Algorithm 1: Algorithmic Steps for ROI Selection.

Data: Structural connectome (66×66), BOLD time series (66×145) for HC and FA

ROI selection using GSP:

1. For every subject in HC and FA,
 - a) Use GFT to extract high/low graph frequency components of BOLD.
 - b) Compute high/low graph frequency energies of graph filtered components of BOLD at all 66 brain regions.
2. For every brain region,
 - a) Perform Mann-Whitney U tests on energies of graph filtered outputs from HC and FA.
 - b) Select the region as ROI if for its Mann-Whitney U test, p -value < 0.05 and effect size > 0.25 .

concentrations for the two groups of subjects in that region were the same. No significant differences in the variances of the distributions of the low or high graph frequency energy concentrations for the two groups of subjects were observed for any brain region.

The Mann-Whitney U test was used to assess whether the region-wise energies of the filtered BOLD signals had different statistical central tendencies across former athletes and healthy controls. The Mann-Whitney U test is a non-parametric test that tests the null hypothesis that the two samples belong to the univariate distributions with same medians against the alternative hypothesis, that they do not, under the assumption that the two distributions being tested have an equal variance. In our study, for every brain region, the null hypothesis was that the corresponding energies of the filtered BOLD signals across each group were drawn from the distributions with similar central tendencies, as opposed to the distributions with different central tendencies in the alternative hypothesis. The test statistic of the Mann-Whitney U test is evaluated based on the number of times the samples from one distribution precedes the samples of the other distribution in the combined sorted arrangement of the samples from the two distributions [63].

To select the regions of interest, we used the p -values for Mann-Whitney U test and the corresponding effect size r based on the z -statistic of the test [64]. The statistical test for a brain region with both p -value < 0.05 and an absolute value of the effect size greater than 0.25 indicated non-trivial statistical differences between the two groups, and therefore, was selected as a region of interest (ROI). A negative effect size for a region indicated that the energy for that region was more likely to be larger for healthy controls than former athletes and vice-versa. The steps for selecting the ROIs using GSP methods described in this section are summarized in Algorithm 1. The statistical significance of the effect sizes was evaluated using a permutation test where the null distribution of effect size for any ROI was generated by randomly shuffling the corresponding graph frequency energy values across the brain regions for every subject and evaluating the effect sizes for the Mann-Whitney U tests for every instance.

We remark that the ROI selection can also be performed based on the ratio of energy of each graph signal contributed by low or high graph frequency components. Additional experiments also indicated that the ROI selection was influenced jointly by structural and functional differences between the two groups (see supplementary file).

C. Dynamic Connectivity Analysis

Dynamic connectivity analysis is often performed on the functional data such as fMRI to analyze the recurring functional connectivity states over the scan length. The sliding window approach is one of the most common methodologies applied for dynamic connectivity analysis (c.f. [20]–[22], [24]–[29]). Furthermore, an ROI based approach is commonly adopted in the brain imaging analysis to isolate the driving features behind the studied phenomenon [65], [66]. In the context of our study, we hypothesized that the ROIs could be informative about any differences between the dynamic connectivity profiles of the two groups of subjects. Therefore, we studied the dynamic connectivity of the high and low graph frequency components from the selected ROIs.

Remark 1: A common fallacy of using an ROI based brain analysis is the statistical bias induced in the results due to non-independence between the process to select the ROIs and the subsequent analysis focused on the selected ROIs [67]. In this paper, we selected the ROIs based on the differences in their respective energy concentrations of graph frequency components in the two groups of subjects. This selection procedure did not provide any information about the correlation among the graph frequency components or their dynamics at the selected ROIs, which is the focus of the dynamic connectivity analysis.

We used a sliding window approach on the graph frequency components of the selected ROIs to find transient connectivity states and characterize the dynamic nature of the graph frequency components of resting state fMRI among a combined set of former athletes and healthy controls. For each subject, we extracted the BOLD signals and their high and low graph frequency components from the ROIs selected using steps from Algorithm 1 over contiguous time windows.

For the results presented in this paper, the length of the time window was fixed at 20 seconds (10 time points) with an overlap of half of the window size between any two consecutive time windows. We calculated a region-wise correlation matrix for each time window which resulted in 28 matrices per subject for all subjects. Correlation matrices from all time windows for all former athletes and healthy controls were pooled for k-means clustering, where the k-means clustering was applied by forming a vector of all pair-wise correlations between different regions for every correlation matrix. The centroids of the identified clusters were associated with the states commonly occurring across former athletes and healthy control subjects. The number of clusters in the k-means clustering algorithm was chosen using Calinski-Harabasz [68] and silhouette [69] criteria, both of which are commonly used to determine the appropriate number of clusters in the dynamic connectivity analysis. We observed that these connectivity states recurred throughout the duration

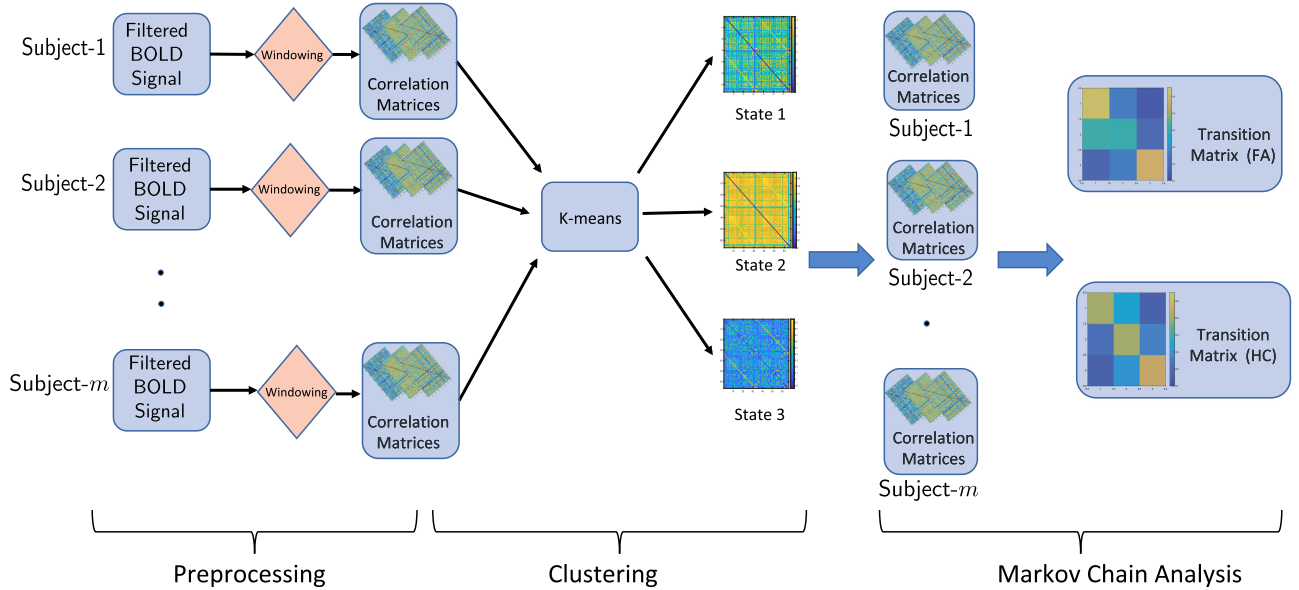


Fig. 5. Illustration of the Multimodal Dynamic Connectivity Analysis for 66 cortical brain regions and 3 states. Graph frequency filters were applied on the BOLD signal in the pre-processing step. HC: Healthy controls, FA: Former athletes.

of the fMRI scans as the brain of each subject switched among different states.

We characterized the dynamic behavior of the brain for healthy controls and former athletes using transition matrices representing the observed instances of the brain switching from one state to another for the two groups. For the k states identified using k-means clustering of correlation matrices, the elements of a transition matrix \mathbf{T}_k of size $k \times k$ were evaluated as

$$[\mathbf{T}_k]_{ij} = \frac{N_{ij}}{\sum_{j=1}^k N_{ij}}, \quad (9)$$

where $[\mathbf{T}_k]_{ij}$ is the (i, j) -th element of \mathbf{T}_k and N_{ij} is the total number of transitions from state i to state j in a given group of subjects. Fig. 5 illustrates the pipeline for the multimodal dynamic connectivity analysis applied for the 66 cortical brain regions. Clearly, the differences in the dynamic connectivity profiles for the two groups of subjects were associated with the states and encoded in the different statistics associated with the Markov chains corresponding to the transition matrices for the two groups. In this paper, we explored the fractions of the total scan time that the brain spends in a particular state for the subjects in the two groups to detect the states with statistically different behavior in the two groups. Specifically, for any subject m , an occupancy ratio OR_i^m was associated with the state $i \in \{1, \dots, k\}$ which quantified the fraction of the total 28 correlation matrices deemed to be associated to that particular state by k-means clustering, i.e.,

$$\text{OR}_i^m \triangleq \frac{\text{Number of matrices in state } i \text{ for subject } m}{28}. \quad (10)$$

We evaluated the ORs for the different states for all subjects in the two groups. The ORs corresponding to different states for the subjects in two groups were evaluated for statistical differences using the Mann-Whitney U test at the significance level of 0.05.

Remark 2: We also remark that the dynamic connectivity analysis results in this paper were robust to the selection of the length of time windows. We observed consistency in the qualitative features of the isolated states (characterized by their respective ORs and the correlation among different brain regions) for the two groups of subjects as the size of the time window was varied from 12 seconds to 32 seconds for the high graph frequency components and from 18 seconds to 28 seconds for the low graph frequency components.

IV. RESULTS

A. GSP Based Regions of Interest

We selected the regions of interest using the steps listed in Algorithm 1. For this purpose, we evaluated the energies of the high graph frequency components of the BOLD time series for all brain regions for all subjects. Fig. 6 plots the p -values of the Mann-Whitney U tests on the high graph frequency energies from healthy subjects and former athletes for different brain regions. Similarly, Fig. 7 plots the p -values of the Mann-Whitney U tests on the high graph frequency energies from healthy subjects and former athletes for different brain regions.

Based on the analysis of the high pass filtered BOLD signal, 5 regions of interest were selected in the left hemisphere for further analysis. The corresponding effect sizes for these ROIs are reported in Table I. No region of interest was selected based on the analysis of high pass filtered BOLD signal in the right hemisphere. Furthermore, based on the analysis of low pass filtered BOLD signal, we selected 4 regions of interest in the right hemisphere, and 4 brain regions of interest in the left hemisphere for further analysis. The corresponding effect sizes for these ROIs are reported in Table II. For the effect sizes associated with the ROIs in Table I and Table II, we also evaluated their statistical significance using a permutation

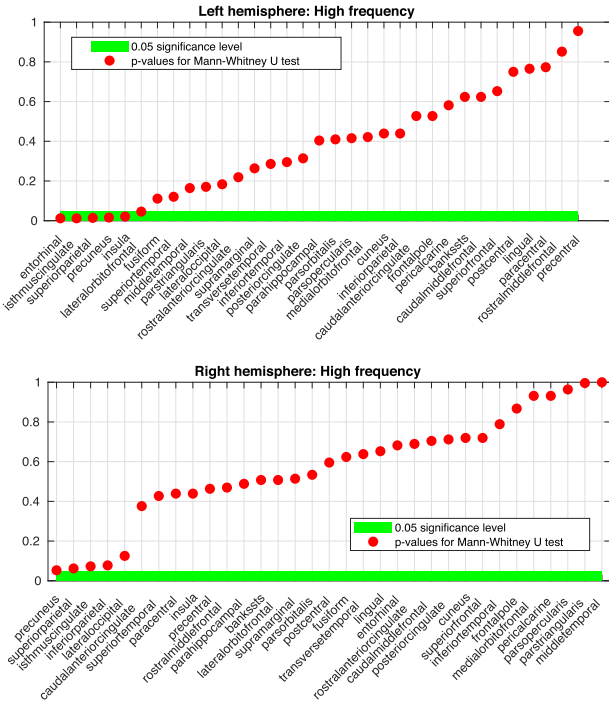


Fig. 6. p -values for Mann-Whitney U test on the energy of high pass filtered BOLD signal from regions in left hemisphere and the right hemisphere.

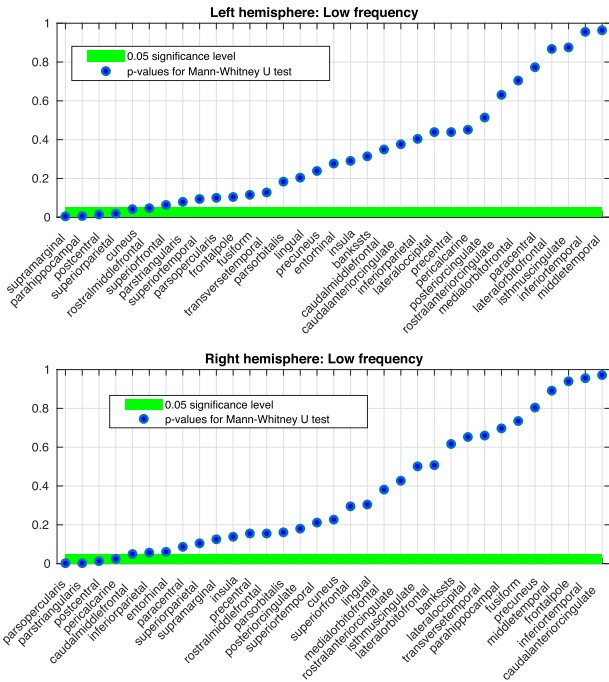


Fig. 7. p -values for Mann-Whitney U test on the energy of low pass filtered BOLD signal from regions in the left hemisphere and the right hemisphere.

based test described in Section III-B3 over a null distribution of effect sizes generated by shuffling the energy values at the brain regions 50000 times for every subject. The p -value for an effect size using this permutation test corresponds to the number of instances for which the observed effect size was strictly greater

TABLE I
ROIS BASED ON HIGH GRAPH FREQUENCY COMPONENTS

ROI	Index	Effect size	p -value (perm. test)
H ₁	ℓ -entorhinal	-0.28	0.0087
H ₂	ℓ -isthmus cingulate	0.279	0.0090
H ₃	ℓ -superior parietal	0.273	0.0115
H ₄	ℓ -precuneus	0.269	0.0129
H ₅	ℓ -insula	-0.257	0.0169

TABLE II
ROIS BASED ON LOW GRAPH FREQUENCY COMPONENTS

Index	ROI	Effect size	p -value (perm. test)
L ₁	ℓ -supramarginal	0.313	0.0045
L ₂	ℓ -para hippocampal	-0.304	0.0054
L ₃	ℓ -postcentral	0.273	0.0142
L ₄	ℓ -superior parietal	0.2613	0.0183
L ₅	r-pericalcarine	-0.251	0.0228
L ₆	r-pars opercularis	0.343	0.0019
L ₇	r-pars triangularis	0.339	0.0017
L ₈	r-postcentral	0.277	0.0122

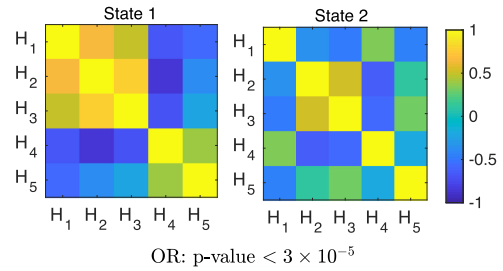


Fig. 8. ROI high graph frequency connectivity states identified based on k-means clustering with 2 clusters. p -values correspond to Mann-Whitney U test on the OR for variation between the two groups of subjects.

than the effect sizes for permuted energy values. For the sake of clarity in subsequent results, we refer to the brain regions of interest by indices listed in Tables I and II, where the prefixes ℓ - and r- are used to indicate that a region is in the left hemisphere and the right hemisphere, respectively. From Tables I and II, we also note that the direction of effects varied across the two groups for different brain regions.

B. Multimodal Dynamic Connectivity Analysis Based on GSP

We restrict the dynamic connectivity analysis to the regions of interest selected using GSP.

1) *High Frequency*: The correlation matrices derived from the time windows of the high frequency components of the BOLD signal in ROIs H₁–H₅ (Table I) for all subjects were pooled together for k-means clustering. Based on the silhouette or the Calinski-Harabasz criteria, the optimal number of clusters was determined to be 7 and 2, respectively. The robustness of the two criteria with respect to the size of the data is discussed in Appendix B. Fig. 8 shows the different states identified based on the dynamic connectivity analysis when the number of clusters is set to 2. The corresponding results for the dynamic connectivity analysis of 7 clusters are presented in Appendix D.

Note that in state 1 in Fig. 8, the high frequency components from ROIs H₁–H₃ are highly correlated with each other while

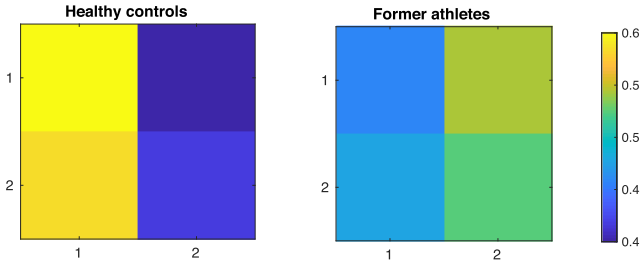


Fig. 9. Transition matrices for a Markov chain based on high graph frequency connectivity states in Fig. 8.

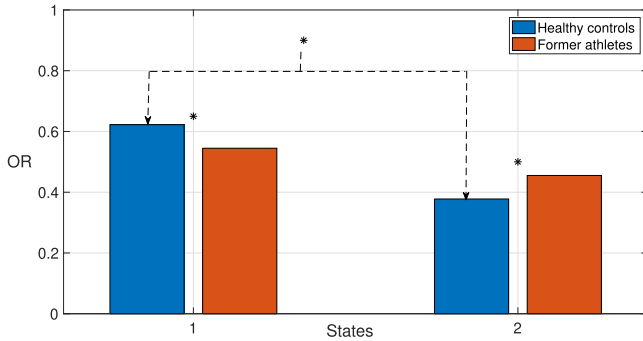


Fig. 10. Mean ORs in the states identified in Fig. 8 for healthy controls and former athletes. Pairs of significantly different ORs between the two groups (Mann-Whitney U test, p -value < 0.05) are marked by an asterisk. The asterisk placed between the blue bar (healthy controls) and red bar (former athletes) for a state indicates that the OR for that state was statistically different for the two groups. Exact p -value is reported in Fig. 8.

being strongly anti-correlated with the high frequency components of the ROIs H_4 and H_5 . This behavior is also observed in state 1 in Fig. 19 in Appendix D where these two states are distinguished by the correlation behavior between the high frequency BOLD signal components for ROIs H_4 (l -precuneus) and H_5 (l -insula). This behavior of the high frequency components of the BOLD time series is not apparent from a general fMRI based dynamic functional connectivity analysis because the higher concentration of lower graph frequency components occlude the effects of the higher graph frequency components in the BOLD time series (see Appendix A for detailed results).

Fig. 9 illustrates the transition matrices for the two state Markov chain formed by states in Fig. 8. Note that the healthy controls tend to stay in state 1 or transition from state 2 to state 1 more frequently as compared to former athletes. This observation is also reflected in the occupancy ratios in Fig. 10 where it is observed that the high frequency functional connectivity for healthy controls dwells longer in state 1 as compared to that for former athletes. Furthermore, the effect size for the Mann-Whitney U test on the OR for the two states in Fig. 10 is 0.476, which indicates a very significant variation in ORs across the two groups of subjects [64]. In addition, the OR in state 1 was significantly higher than that for state 2 for healthy controls (Mann-Whitney U test: p -value $< 9 \times 10^{-8}$, effect size = 0.596). In contrast, we did not find significant variation between the ORs in state 1 and state 2 for former athletes (Mann-Whitney U test: p -value > 0.9 , effect size < 0.01) or for the

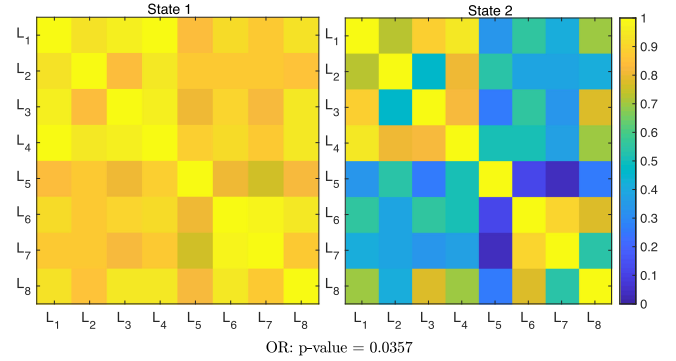


Fig. 11. ROI low graph frequency connectivity states identified based on k -means clustering with 2 clusters. p -values correspond to Mann-Whitney U test on the OR for variation between the two groups of subjects.

combined cohort consisting of the two groups (Mann-Whitney U test: p -value > 0.2 , effect size = 0.136).

In this section, we focused on the results corresponding to 2 clusters. We also observed that the results presented in this section were robust with respect to the number of ROIs used in the analysis as well as the addition of other brain regions. See Appendix C for more details.

2) *Low Frequency*: We performed the dynamic analysis based on the low graph frequency components of the BOLD signals from the ROIs L_1 – L_8 (Table II). Based on the silhouette or the Calinski-Harabasz criteria, the optimal number of clusters was determined to be 2 and 3, respectively. In this section, we focus on the results corresponding to two clusters. The results for three clusters are included in Appendix E. Fig. 11 shows the different states identified based on the dynamic connectivity analysis when the number of clusters is set to 2.

Note that state 1 in Fig. 11 represents the highly correlated low frequency functional connectivity across the 8 ROIs. Since the low graph frequency filter isolates the spatially smooth components of the BOLD time series over the graph, the presence of this state is expected. Similarly, we observe a highly correlated state (State 1) in Fig. 22 when the dynamic connectivity analysis is performed for 3 states.

Fig. 12 shows the mean occupancy ratios for healthy controls and former athletes for the two state Markov chain formed by the states in Fig. 11. Note that for both groups of subjects, the low frequency functional connectivity based on ROIs L_1 – L_8 tends to stay in state 1 significantly more frequently as compared to state 2 (Mann-Whitney U test: p -value $< 4 \times 10^{-25}$, effect size = 1.224). This is expected because low pass graph filter isolates the components of the graph signal (in this case, BOLD signal) that are driven by the edge connectivity of the graph. However, the comparison of occupancy ratios for state 1 for the two groups using Mann-Whitney U test suggests that the low graph frequency functional connectivity for healthy controls spends significantly more time in the highly correlated state 1 as compared to that for former athletes (p -value = 0.0357, effect size = 0.24). We also observed that the results presented in this section were robust with respect to the number of ROIs used in the analysis as well as the addition of other brain regions. See the supplementary file for more details.

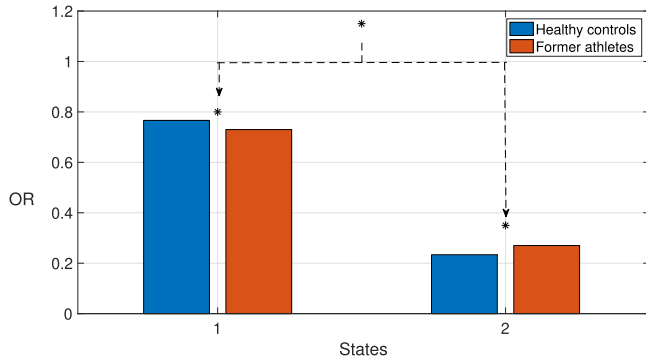


Fig. 12. Mean ORs in the states identified in Fig. 11 for healthy controls and former athletes. Pairs of significantly different ORs between the two groups (Mann-Whitney U test, p -value < 0.05) are marked by an asterisk. The asterisk placed between the blue bar (healthy controls) and red bar (former athletes) for a state indicates that the OR for that state was statistically different for the two groups. Exact p -value is reported in Fig. 10. Both groups of subjects had a significantly higher OR in State 1 as compared to State 2 (marked by the asterisk between the two states).

V. DISCUSSION

The results in Section IV summarized the different recurring graph frequency based functional connectivity states and the comparison of their respective ORs between former athletes and healthy controls. To the best of our knowledge, the use of high/low graph frequency components for dynamic connectivity analysis is novel. Our results showed that the fractions of the time spent in some states over the scan length were significantly different for the two groups of subjects. Therefore, the results indicate that the features could be used to discriminate between healthy subjects and former athletes.

We also briefly discuss the results presented in Section IV from the anatomical and clinical perspective. Using the high graph frequency and low graph frequency analysis, 13 cortical brain regions were selected as ROIs. Notably, only one cortical region (superior parietal in left hemisphere) was selected as an ROI from the analysis of both the low graph frequency and the high graph frequency components of the BOLD signal. In general, the individuals with a history of multiple concussions are vulnerable to cognitive impairments linked with irritability, aggression, anxiety, and depression [70]. Furthermore, the regions in the frontal and temporal lobes are more vulnerable to injury due to their location [71]. In this context, the brain regions selected as ROIs in this paper are relevant. The regions insula and precuneus have been linked with anxiety disorders [72], hippocampus and entorhinal with depression [73], and postcentral, supramarginal and para hippocampal with panic disorders [74]. Therefore, it is of interest to investigate if the features isolated in this paper correlate with behavioral metrics of former athletes. These observations also raise the question whether the states isolated in the dynamic connectivity analysis are indicative of vulnerabilities of the human brain to cognitive impairments.

Furthermore, the ROIs in this paper have also been isolated as affected brain regions in the existing studies on TBI and its neurocognitive effects [75]–[80]. The regions in inferior frontal gyrus have been previously identified as regions with

altered functional connectivity in the studies on athletes with a history of concussions [75], [76]. Precuneus was identified as a region of interest based on the structural and functional connectivity analysis in [76], [77]. Significant reduction in white matter volume of isthmus cingulate for subjects with mTBI was reported in [78] and correlated with neurocognitive metrics on anxiety and depression. l -superior parietal was identified as a region of interest based on the analysis of fMRI and working memory performance in [79]. Limbic regions were identified as the focal points of study of cognitive dysfunction due to TBI in [80]. The progression of the neurocognitive problems in subjects with TBI to neurodegenerative diseases, e.g. chronic traumatic encephalopathy (CTE), is another direction of research [81]–[83]. The regions l -supramarginal, l -postcentral, and l -precuneus have also been identified as regions of interest showing alterations in the existing studies on CTE [84]–[86].

Next we comment on the perpetual and a few transitional functional relationships among different cortical brain regions based on the analysis of the high graph frequency functional connectivity states in Fig. 8 and those in Fig. 19 in Appendix D based on 7 clusters, and the low graph frequency functional connectivity states in Fig. 11 and those in Fig. 22 in Appendix E.

The high graph frequency components of the BOLD signal in the regions l -entorhinal (H_1) and l -isthmus cingulate (H_2) in the limbic lobe and l -superior parietal (H_3) in the parietal lobe have high positive correlation in state 1 in Fig. 8 and states 1 and 3 in Fig. 19. From Fig. 10 and Fig. 21, we conclude that the highly correlated behavior among the regions H_1 – H_3 that characterizes these states is more frequent in healthy controls than former athletes. In contrast, l -superior parietal (H_3) has positive high graph frequency functional connectivity with l -isthmus cingulate (H_2) and negative high graph frequency functional connectivity with l -entorhinal (H_1) in state 2 in Fig. 8 and states 6 and 7 in Fig. 19.

The high graph frequency components of the BOLD signals from the regions l -superior parietal (H_3) and l -precuneus (H_4) in the parietal lobe are anti-correlated across both states in Fig. 8 and states 1, 3, 5, 6 and 7 in Fig. 19. The high graph frequency components of the BOLD signal from l -insula (H_5) were anti-correlated with that from l -entorhinal (H_1) in states 1 and 2 in Fig. 8 and states 1, 2, 4, 5, and 7 in Fig. 19. The anti-correlation behavior among the regions H_1 – H_5 is not as distinctly observed in the dynamic connectivity analysis of unfiltered fMRI (see Appendix A).

The regions r-pars opercularis (L_6) and r-pars triangularis (L_7) in the inferior frontal gyrus of the frontal lobe were selected as ROIs based on low graph frequency dynamic functional connectivity analysis. Also, the low graph frequency components of the BOLD signals from both regions were significantly correlated across all isolated states in Fig. 11 and Fig. 22.

r-pericalcarine (L_5) was the only region in the occipital lobe that was selected as an ROI. Note that in the state 2 in Fig. 11 and state 2 in Fig. 22, the low graph frequency component of the BOLD signal from r-pericalcarine (L_5) was almost uncorrelated with that from the regions in the inferior frontal gyrus (L_6 and L_7). This uncorrelated behavior was observed more frequently in former athletes than healthy controls (Fig. 12 and Fig. 24).

Postcentral in the parietal lobe was selected as an ROI in both brain hemispheres. It is interesting to note that ℓ -postcentral (L_3) and r-postcentral (L_8) had distinct characteristics across the isolated states in Fig. 11 and Fig. 22. The regions ℓ -supramarginal (L_1) and ℓ -superior parietal (L_4) in the parietal lobe in the left hemisphere had high positive correlation with ℓ -postcentral (L_3) across all states in Fig. 11 and Fig. 22. On the other hand, the low graph frequency functional connectivity for r-postcentral (L_8) had a weaker correlation with that from ℓ -supramarginal (L_1), and ℓ -superior parietal (L_4) as compared to that between ℓ -postcentral (L_3) and these regions in state 3 in Fig. 22. The low graph frequency component of the BOLD signal from ℓ -para hippocampal (L_2) had high positive correlation with that from ℓ -supramarginal (L_1) and ℓ -superior parietal (L_4) in the parietal lobe across all states in Fig. 11 and Fig. 22.

VI. CONCLUSION

We have applied a multimodal dynamic functional connectivity framework to analyze the brain imaging data collected from a population of former athletes with a history of multiple concussions and healthy controls with no reported history of concussion. The brain regions with non trivial statistical variations in the high/low graph frequency components of the BOLD signal in former athletes and healthy controls have been selected as regions of interest. A sliding window dynamic connectivity analysis approach has been applied on the *graph filtered* BOLD signal from the regions of interest and different functional connectivity states have been determined. Significantly different dwell times for healthy controls and former athletes were observed for multiple functional connectivity states. The structure of the functional connectivity states have been studied and elaborated on from the anatomical perspective. A brief review of existing clinical studies on TBI has revealed that the ROIs identified in this paper correlate with cognitive dysfunction, task-related performance and neurodegeneration.

ACKNOWLEDGMENT

The authors are indebted to Sushmita Allam for helpful discussions on the statistical assessments.

APPENDIX A UNIMODAL DYNAMIC CONNECTIVITY ANALYSIS OF REGIONS H_1 – H_5

We used the unfiltered fMRI BOLD time series for the unimodal dynamic connectivity analysis. Based on the Calinski-Harabasz or the silhouette criteria, the optimal number of clusters were determined to be 2 and 4, respectively.

Figs. 13 and 15 illustrate the dynamic connectivity states identified using unimodal dynamic connectivity analysis where the number of clusters in k-means clustering step was set to 2 and 4, respectively.

Note that the state 1 in Fig. 13 and state 4 in Fig. 15 are qualitatively similar, i.e., the ROIs H_1 – H_5 are comparatively more functionally co-activated as compared to the other isolated states. We tabulate the main observations from the comparison of the results in this section and Section IV-B1.

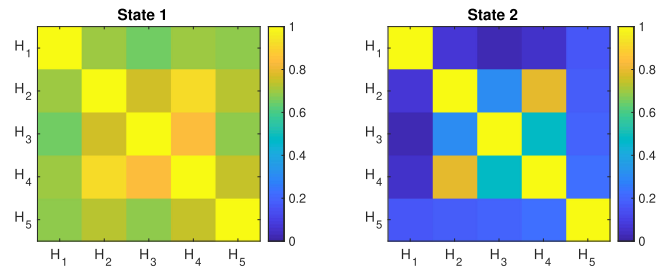


Fig. 13. ROI functional connectivity states identified without the application of graph frequency filter on BOLD signal. The number of clusters in k-means was set to 2.

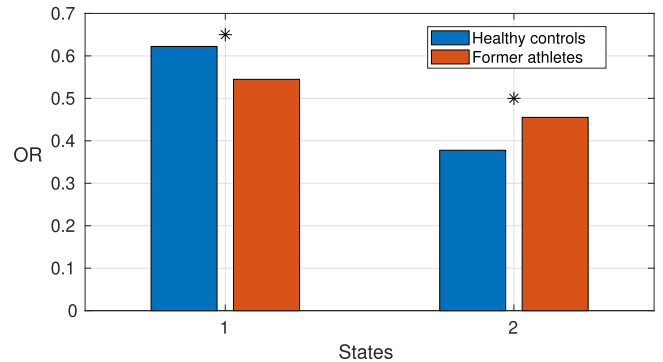


Fig. 14. Mean ORs in the states identified in Fig. 13 for healthy controls and former athletes. Pairs of significantly different ORs between the two groups (Mann-Whitney U test, p -value < 0.05) are marked by an asterisk. The asterisk placed between the blue bar (healthy controls) and red bar (former athletes) for a state indicates that the OR for that state was statistically different for the two groups.

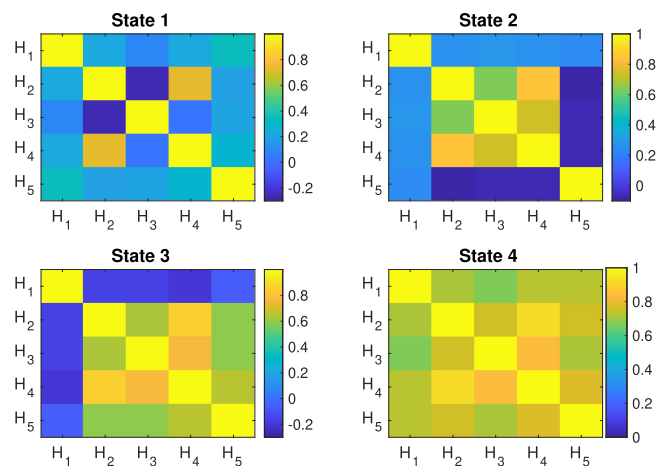


Fig. 15. ROI functional connectivity states identified without the application of graph frequency filter on BOLD signal. The number of clusters in k-means was set to 4.

- 1) The analysis of OR in Fig. 14 and Fig. 16 reveals that the healthy controls tend to stay longer in this highly correlated state as compared to former athletes. This behavior, although similar to the one observed in the analysis of low frequency based ROIs L_1 – L_8 , is not corroborated by the

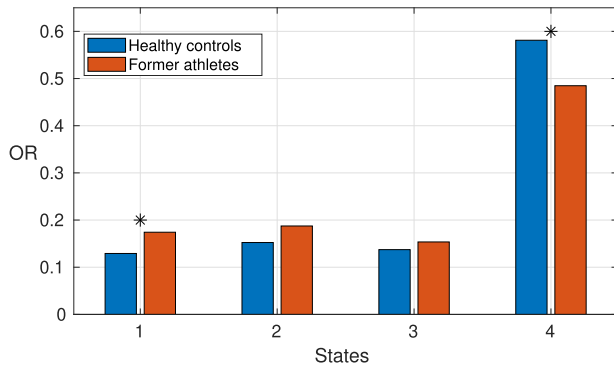


Fig. 16. Mean ORs in the states identified in Fig. 15 for healthy controls and former athletes. Pairs of significantly different ORs between the two groups (Mann-Whitney U test, p -value < 0.05) are marked by an asterisk. The asterisk placed between the blue bar (healthy controls) and red bar (former athletes) for a state indicates that the OR for that state was statistically different for the two groups.

analysis of the low graph frequency components of the BOLD signal from the regions $H_1 - H_5$.

- Note that although the functional connectivity varies significantly across the states 1-4 in Fig. 15, we do not observe the highly anti-correlated behavior among different brain regions revealed in the analysis of the high frequency BOLD signal in Section IV-B1.

Both the observations listed above suggest that GSP based multimodal dynamic connectivity analysis of the BOLD signal helps amplify the differences in the functional connectivity between the two groups of subjects and also isolate the unique functional connectivity behavior that may not be evident from the unimodal dynamic connectivity analysis.

APPENDIX B

ROBUSTNESS OF CALINKSI-HARABASZ AND SILHOUETTE CRITERIA FOR HIGH GRAPH FREQUENCY COMPONENTS

To check the robustness of the optimal number of clusters for the two criteria, we evaluated the optimal number of clusters for random instances of smaller sized data. Note that the complete data consisted of 2268 correlation matrices (81 subjects, 28 correlation matrices per subject) that were clustered using k-means algorithm. We evaluated the silhouette and the Calinski-Harabasz criteria for 100 random selections of 1200, 1400, 1600, 1800 or 2200 correlation matrices.

Note that the silhouette criterion quantifies the similarity of the items with their assigned cluster with respect to the items from any other cluster. Therefore, the optimal number of clusters based on the silhouette criterion is determined by the highest observed silhouette index. Fig. 17 illustrates the variation of silhouette index with the number of clusters for different sizes of the data used for k-means clustering. We consistently observe the maxima of the silhouette index at $k = 7$ which indicates that the optimal number of clusters selected based on the complete data is robust.

We run similar analysis to check the robustness of the optimal number of clusters obtained based on the Calinski-Harabasz criterion. Note that the index for the Calinski-Harabasz criterion

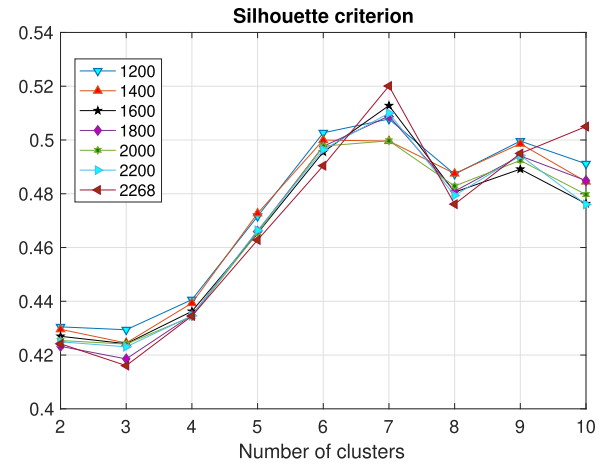


Fig. 17. Silhouette index vs number of clusters for different data size. The silhouette indices for any data size < 2268 are determined by averaging over 100 random selections of the data samples of the given size.

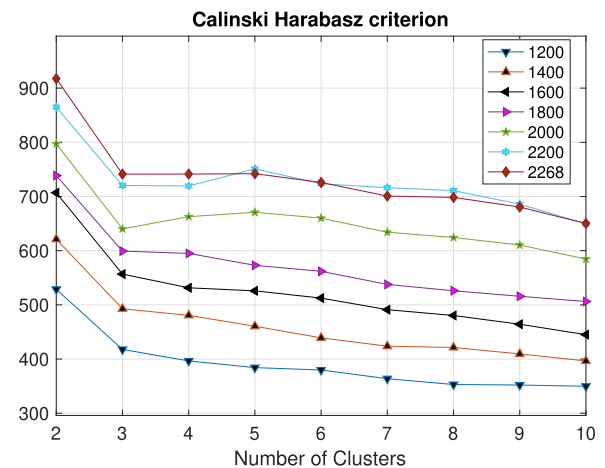


Fig. 18. Calinski-Harabasz index vs number of clusters for different data size. The silhouette indices for any data size < 2268 are determined by averaging over 100 random selections of the data samples of the given size.

depends on the ratio of the overall between cluster variance, i.e., the sum of variances of the items in different clusters, and the overall within cluster variance, i.e., the sum of the variances of the items assigned to the same clusters. Therefore, the optimal number of clusters based on the Calinski-Harabasz criterion correspond to the highest Calinski-Harabasz index. Fig. 18 illustrates the variation of Calinski-Harabasz index with the number of clusters for different sizes of the data used for k-means clustering. We consistently observe the maxima of the index at $k = 2$ which indicates that the optimal number of clusters selected based on the complete data is robust.

APPENDIX C

ROBUSTNESS OF DYNAMIC CONNECTIVITY RESULTS FOR $H_1 - H_5$

We checked the robustness of the dynamic connectivity analysis results against the number of ROIs used in the analysis and addition of other brain regions. Here we list the results

TABLE III
 p -VALUES FOR MANN-WHITNEY U TEST BETWEEN THE ORS FOR 4 ROIS
 FROM H_1-H_5

ROI	p -value
H_1, H_2, H_3, H_4	6.54×10^{-5}
H_1, H_2, H_3, H_5	3.66×10^{-6}
H_1, H_2, H_4, H_5	3.84×10^{-5}
H_1, H_3, H_4, H_5	0.0017
H_2, H_3, H_4, H_5	7.16×10^{-9}

TABLE IV
 p -VALUES FOR MANN-WHITNEY U TEST BETWEEN THE ORS FOR 3 ROIS
 FROM H_1-H_5

ROI	p -value
H_1, H_2, H_3	0.0014
H_1, H_2, H_4	1.61×10^{-4}
H_1, H_2, H_5	2.2×10^{-4}
H_1, H_3, H_4	0.0058
H_1, H_3, H_5	0.0026
H_1, H_4, H_5	0.0193
H_2, H_3, H_4	4.08×10^{-9}
H_2, H_3, H_5	1.39×10^{-6}
H_2, H_4, H_5	8.75×10^{-5}
H_3, H_4, H_5	1.72×10^{-5}

establishing the robustness of the dynamic connectivity analysis based on 2 states for ROIs H_1-H_5 .

- a) *Robustness against less number of regions:* Tables III and IV list the p -values of the Mann-Whitney U tests on the ORs for healthy subjects and former athletes evaluated by different permutations of 4 and 3 ROIs, respectively. Clearly, the results obtained by using different combinations of 3 or 4 ROIs are statistically significant (p -value < 0.05) which indicates the robustness of the dynamic connectivity analysis with respect to the selection of ROIs.
- b) *Robustness against additional brain regions:* Next, we evaluated the robustness of the dynamic connectivity analysis results against the use of 1 or 2 brain regions in addition to the selected ROIs. For all 61 brain regions that were not ROIs H_1-H_5 , we evaluated the statistical significance of the dynamic connectivity analysis results after adding their respective high graph frequency components to the analysis one at a time or two at a time. For the addition of one brain region to the ROIs for dynamic connectivity analysis, we observed that the results were statistically significant at the level of p -value < 0.05 for 59 brain regions, at the level of p -value $< 10^{-3}$ for 49 brain regions, and at the level of p -value $< 10^{-5}$ for 21 brain regions. The dynamic connectivity results were not statistically significant (p -value > 0.05) for the ROIs and an additional brain region which was either ℓ -posterior cingulate or ℓ -rostral anterior cingulate.

We also evaluated the statistical significance of the dynamic connectivity analysis results for ROIs and two additional brain regions. The two additional brain regions could be selected in $\binom{61}{2} = 1830$ number of ways. Our experiments revealed that the results for dynamic connectivity analysis in terms of the comparison of OR between the two groups were statistically significant at the level of p -value < 0.05

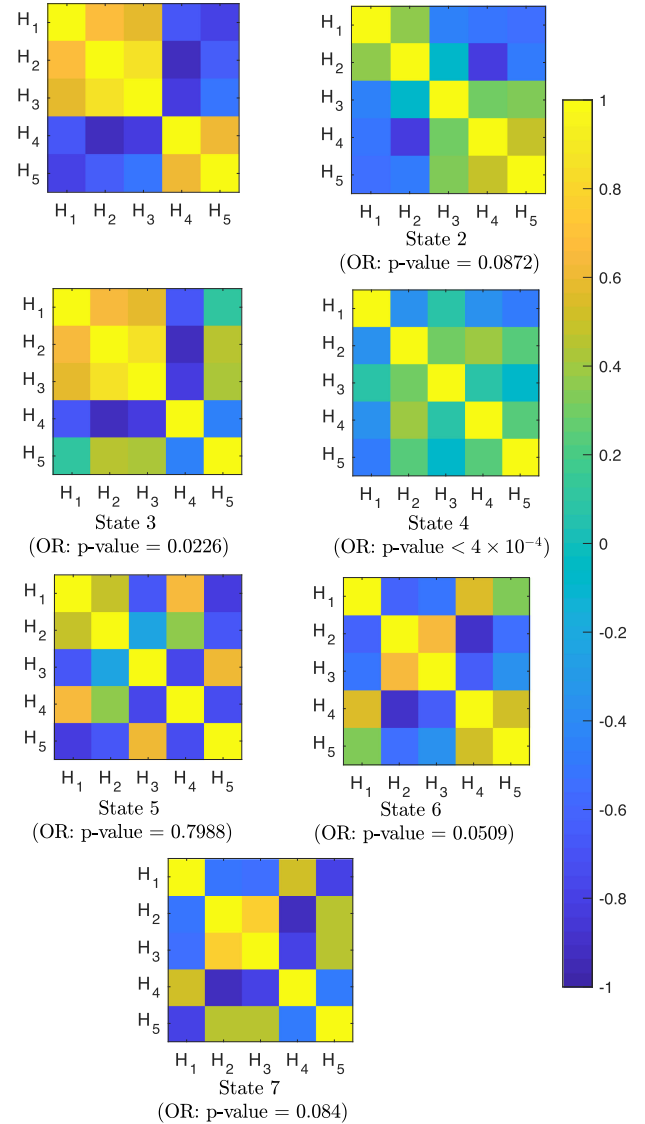


Fig. 19. ROI high graph frequency connectivity states identified based on k-means clustering with 7 clusters. p -values correspond to Mann-Whitney U test on the OR for variation between the two groups of subjects and were corrected for multiple comparisons [87].

for 1676 pairs (91.58% of 1830). Therefore, our experiments illustrate that the results for the dynamic connectivity analysis for the ROIs selected using graph filtering operations were robust to the selection of additional 1 or 2 brain regions.

APPENDIX D DYNAMIC CONNECTIVITY ANALYSIS FOR HIGH GRAPH FREQUENCY COMPONENTS WITH 7 CLUSTERS

Fig. 19 shows the different states identified based on the dynamic connectivity analysis when the number of clusters is set to 7. Fig. 20 illustrates the transition matrices for the 7 state Markov chain formed by states in Fig. 19 and their respective p -values for the Mann-Whitney U test on the ORs for the two groups. The p -values reported in Fig. 20 were corrected for

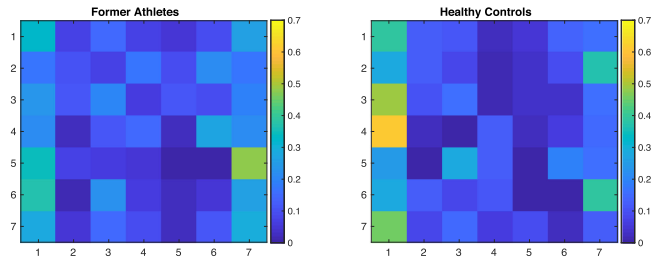


Fig. 20. Transition matrices for a Markov chain based on 7 high graph frequency connectivity states in Fig. 19.

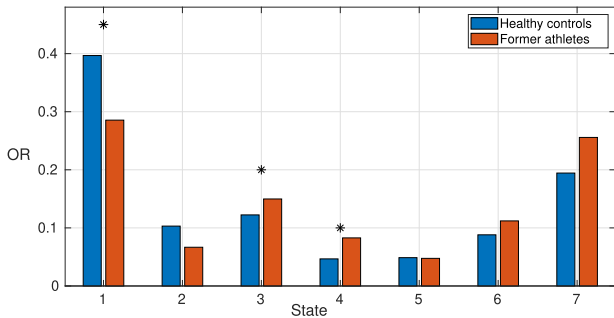


Fig. 21. Mean ORs in the states identified in Fig. 19 for healthy controls and former athletes. Pairs of significantly different ORs between the two groups (Mann-Whitney U test, p -value < 0.05) are marked by an asterisk. Exact p -values are reported in Fig. 19. Significance tests for differences between the ORs for individual states were not performed.

multiple comparison using false discovery rate method [87]. Note that the healthy controls tend to stay in state 1 or transition from other states to state 1 more frequently as compared to former athletes. This observation is also reflected in the occupancy ratios in Fig. 21 where it is observed that the high frequency functional connectivity for healthy controls dwells longer in state 1 as compared to that for former athletes. The effect sizes for the Mann-Whitney U test on the ORs for state 1, state 3, and state 4 in Fig. 21 are -0.595 , 0.248 , and 0.43 , respectively, indicating a significant variation in ORs across the two groups of subjects [64]. Note that a negative effect size for the comparison of the OR for a particular state between the two groups indicates that the healthy controls have a significantly higher OR in that state as compared to that for former athletes.

APPENDIX E

DYNAMIC CONNECTIVITY ANALYSIS WITH 3 CLUSTERS FOR LOW GRAPH FREQUENCY COMPONENTS FROM ROIS

Fig. 22 shows the different states identified based on the dynamic connectivity analysis when the number of clusters is set to 3. State 1 in Fig. 22 represents the highly correlated low frequency functional connectivity across the 8 ROIs which is similar to state 1 in Fig. 11. Fig. 23 illustrates the transition matrices for the two groups of subjects with respect to a Markov chain formed by the states in Fig. 22. Fig. 24 shows that the highly correlated state 1 in Fig. 22 has a significantly lower OR (p -value < 0.05 , effect size = -0.284) for former athletes as

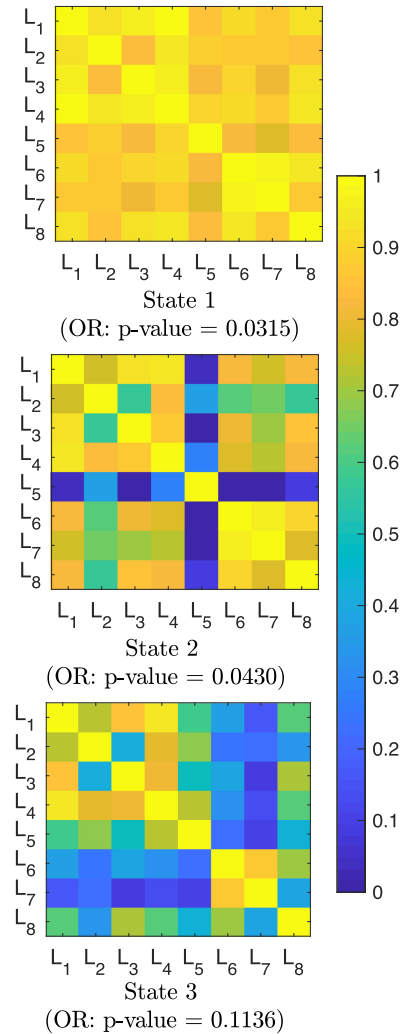


Fig. 22. ROI low graph frequency connectivity states identified based on k -means clustering with 3 clusters. p -values correspond to Mann-Whitney U test on the OR for variation between the two groups of subjects and were corrected for multiple comparisons [87].

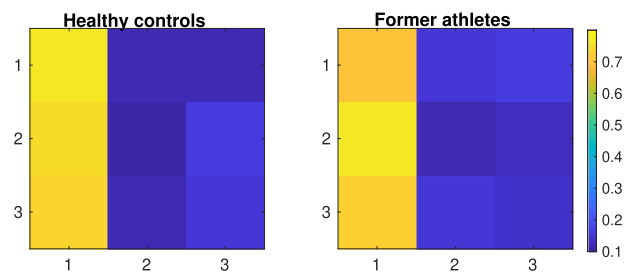


Fig. 23. Transition matrices for a Markov chain based on 3 low graph frequency connectivity states in Fig. 22.

compared to healthy controls. This observation is in line with the observations based on the analysis of the 2 state Markov chain formed by the states in Fig. 11. Clearly, the low frequency components of the BOLD signal for the ROIs are characterized by less frequent highly correlated states in former athletes as compared to healthy controls.

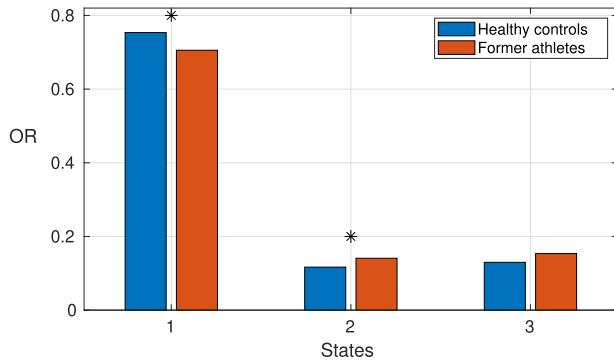


Fig. 24. Mean ORs in the states identified in Fig. 22 for healthy controls and former athletes. Pairs of significantly different ORs between the two groups (Mann-Whitney U test, p -value < 0.05) are marked by an asterisk. Significance tests for differences between the ORs for individual states were not performed.

REFERENCES

- [1] E. Bullmore and O. Sporns, "Complex brain networks: Graph theoretical analysis of structural and functional systems," *Nature Reviews Neurosci.*, vol. 10, pp. 186–198, Feb. 2009.
- [2] E. T. Bullmore and D. S. Bassett, "Brain graphs: Graphical models of the human brain connectome," *Annu. Rev. Clin. Psychology*, vol. 7, pp. 113–140, Apr. 2011.
- [3] O. Sporns, *Networks of the Brain*. Cambridge, MA, USA: MIT Press, 2010.
- [4] V. D. Calhoun, R. Miller, G. Pearlson, and T. Adali, "The chronnectome: Time-varying connectivity networks as the next frontier in fMRI data discovery," *Neuron*, vol. 84, no. 2, pp. 262–274, 2014.
- [5] D. A. Handwerker, V. Roopchansingh, J. Gonzalez-Castillo, and P. A. Bandettini, "Periodic changes in fMRI connectivity," *NeuroImage*, vol. 63, no. 3, pp. 1712–1719, Nov. 2012.
- [6] K. Li, L. Guo, J. Nie, G. Li, and T. Liu, "Review of methods for functional brain connectivity detection using fMRI," *Computerized Med. Imag. Graph.*, vol. 33, no. 2, pp. 131–139, 2009.
- [7] F. Mokhtari, M. I. Akhlaghi, S. L. Simpson, G. Wu, and P. J. Laurienti, "Sliding window correlation analysis: Modulating window shape for dynamic brain connectivity in resting state," *Neuroimage*, vol. 189, pp. 655–666, Apr. 2019.
- [8] E. A. Allen, E. Damaraju, S. M. Plis, E. B. Erhardt, T. Eichele, and V. D. Calhoun, "Tracking whole-brain connectivity dynamics in the resting state," *Cerebral Cortex*, vol. 24, no. 3, pp. 663–676, Mar. 2014.
- [9] A. Liu, X. Chen, X. Dan, M. J. McKeown, and Z. J. Wang, "A combined static and dynamic model for resting-state brain connectivity networks," *IEEE J. Sel. Topics Signal Process.*, vol. 10, no. 7, pp. 1172–1181, Oct. 2016.
- [10] B. Cai *et al.*, "Capturing dynamic connectivity from resting state fMRI using time-varying graphical lasso," *IEEE Trans. Biomed. Eng.*, vol. 66, no. 7, pp. 1852–1862, Jul. 2019.
- [11] A. Ozdemir, E. M. Bernat, and S. Aviyente, "Recursive tensor subspace tracking for dynamic brain network analysis," *IEEE Trans. Signal Inf. Process. Over Netw.*, vol. 3, no. 4, pp. 669–682, Dec. 2017.
- [12] R. Warnick, M. Guindani, E. Erhardt, E. Allen, V. Calhoun, and M. Vannucci, "A Bayesian approach for estimating dynamic functional network connectivity in fMRI data," *J. Amer. Statistical Assoc.*, vol. 113, no. 521, pp. 134–151, Jan. 2018.
- [13] M. Pedersen, A. Omidvarnia, A. Zalesky, and G. D. Jackson, "On the relationship between instantaneous phase synchrony and correlation-based sliding windows for time-resolved fMRI connectivity analysis," *Neuroimage*, vol. 181, pp. 85–94, Nov. 2018.
- [14] N. Leonardi *et al.*, "Principal components of functional connectivity: A new approach to study dynamic brain connectivity during rest," *NeuroImage*, vol. 83, pp. 937–950, 2013.
- [15] Q. Yu *et al.*, "Application of graph theory to assess static and dynamic brain connectivity: Approaches for building brain graphs," *Proc. IEEE*, vol. 106, no. 5, pp. 886–906, May 2018.
- [16] E. Tagliazucchi and H. Laufs, "Multimodal imaging of dynamic functional connectivity," *Frontiers Neurol.*, vol. 6, p. 10, 2015.
- [17] M. Kudela, J. Harezlak, and M. A. Lindquist, "Assessing uncertainty in dynamic functional connectivity," *NeuroImage*, vol. 149, pp. 165–177, Apr. 2017.
- [18] A. Córdova-Palamera *et al.*, "Disrupted global metastability and static and dynamic brain connectivity across individuals in the Alzheimer's disease continuum," *Scientific Rep.*, vol. 7, Jan. 2017, Art. no. 40268.
- [19] Q. Yu *et al.*, "Assessing dynamic brain graphs of time-varying connectivity in fMRI data: application to healthy controls and patients with schizophrenia," *NeuroImage*, vol. 107, pp. 345–355, Feb. 2015.
- [20] E. Damaraju *et al.*, "Dynamic functional connectivity analysis reveals transient states of dysconnectivity in schizophrenia," *NeuroImage: Clinical*, vol. 5, pp. 298–308, 2014.
- [21] S. Ma, V. D. Calhoun, R. Phlypo, and T. Adali, "Dynamic changes of spatial functional network connectivity in healthy individuals and Schizophrenia patients using independent vector analysis," *NeuroImage*, vol. 90, pp. 196–206, Apr. 2014.
- [22] J. M. Reinen *et al.*, "The human cortex possesses a reconfigurable dynamic network architecture that is disrupted in psychosis," *Nature Commun.*, vol. 9, no. 1, pp. 1–15, Mar. 2018.
- [23] C. Luo *et al.*, "Disrupted functional brain connectivity in partial epilepsy: A resting-state fMRI study," *PLoS One*, vol. 7, no. 1, Jan. 2012, Art. no. e28196.
- [24] R. Li *et al.*, "Differential patterns of dynamic functional connectivity variability of striato-cortical circuitry in children with benign epilepsy with centrotemporal spikes," *Human Brain Mapping*, vol. 39, no. 3, pp. 1207–1217, 2018.
- [25] F. Mokhtari *et al.*, "Dynamic fMRI networks predict success in a behavioral weight loss program among older adults," *NeuroImage*, vol. 173, pp. 421–433, 2018.
- [26] G. Engels, A. Vlaar, B. McCoy, E. Scherder, and L. Douw, "Dynamic functional connectivity and symptoms of Parkinson's disease: A resting-state fMRI study," *Frontiers Aging Neurosci.*, vol. 10, 2018.
- [27] R. H. Kaiser *et al.*, "Dynamic resting-state functional connectivity in major depression," *Neuropsychopharmacology*, vol. 41, pp. 1822–1830, Dec. 2015.
- [28] A. R. Mayer, J. M. Ling, E. A. Allen, S. D. Klimaj, R. A. Yeo, and F. M. Hanlon, "Static and dynamic intrinsic connectivity following mild traumatic brain injury," *J. Neurotrauma*, vol. 32, no. 14, pp. 1046–1055, Jul. 2015.
- [29] Vergara, V. M., A. R. Mayer, E. Damaraju, and V. D. Calhoun, "The effect of preprocessing in dynamic functional network connectivity used to classify mild traumatic brain injury," *Brain Behav.*, vol. 7, no. 10, Oct. 2017, Art. no. e00809.
- [30] W. Hou *et al.*, "Dynamic functional network analysis in mild traumatic brain injury," *Brain Connectivity*, vol. 9, Apr. 2019, pp. 475–487.
- [31] P. J. A. Dean, J. R. Sato, G. Vieira, A. McNamara, and A. Sterr, "Multimodal imaging of mild traumatic brain injury and persistent postconcussion syndrome," *Brain Behav.*, vol. 5, no. 1, Dec. 2015, Art. no. e00292.
- [32] C. Cao and S. Slobounov, "Alteration of cortical functional connectivity as a result of traumatic brain injury revealed by graph theory, ICA, and sLORETA analyses of EEG signals," *IEEE Trans. Neural Syst. Rehabil. Eng.*, vol. 18, no. 1, pp. 11–19, Feb. 2010.
- [33] T. Nakamura, F. G. Hillary, and B. B. Biswal, "Resting network plasticity following brain injury," *PLOS One*, vol. 4, no. 12, pp. 1–9, Dec. 2009.
- [34] D. J. Sharp, G. Scott, and R. Leech, "Network dysfunction after traumatic brain injury," *Nature Rev. Neurol.*, vol. 10, pp. 156–166, Feb. 2014.
- [35] W. Yuan, S. L. Wade, and L. Babcock, "Structural connectivity abnormality in children with acute mild traumatic brain injury using graph theoretical analysis," *Human Brain Mapping*, vol. 36, no. 2, pp. 779–792, 2015.
- [36] A. Messé *et al.*, "Specific and evolving resting-state network alterations in post-concussion syndrome following mild traumatic brain injury," *PLOS ONE*, vol. 8, no. 6, pp. 1–10, Jun. 2013.
- [37] K. Caeyenberghs *et al.*, "Altered structural networks and executive deficits in traumatic brain injury patients," *Brain Struct. Function*, vol. 219, no. 1, pp. 193–209, Jan. 2014.
- [38] V. M. Vergara, A. R. Mayer, E. Damaraju, K. A. Kiehl, and V. Calhoun, "Detection of mild traumatic brain injury by machine learning classification using resting state functional network connectivity and fractional anisotropy," *J. Neurotrauma*, vol. 34, no. 5, pp. 1045–1053, Mar. 2017.
- [39] V. D. Calhoun and J. Sui, "Multimodal fusion of brain imaging data: A key to finding the missing link(s) in complex mental illness," *Biol. Psychiatry: Cogn. Neurosci. Neuroimag.*, vol. 1, no. 3, pp. 230–244, 2016.
- [40] A. R. Mayer *et al.*, "A functional MRI study of multimodal selective attention following mild traumatic brain injury," *Brain Imag. Behav.*, vol. 6, no. 2, pp. 343–354, Jun. 2012.

- [41] T. Babikian *et al.*, "Metabolic levels in the corpus callosum and their structural and behavioral correlates after moderate to severe pediatric TBI," *J. Neurotrauma*, vol. 27, no. 3, pp. 473–481, Mar. 2010.
- [42] K. Caeyenberghs *et al.*, "Graph analysis of functional brain networks for cognitive control of action in traumatic brain injury," *Brain*, vol. 135, no. 4, pp. 1293–1307, 2012.
- [43] N. Churchill, M. Hutchison, D. Richards, G. Leung, S. Graham, and T. A. Schweizer, "Brain structure and function associated with a history of sport concussion: A multi-modal magnetic resonance imaging study," *J. Neurotrauma*, vol. 34, no. 4, pp. 765–771, Feb. 2017.
- [44] T. Itahashi *et al.*, "Linked alterations in gray and white matter morphology in adults with high-functioning autism spectrum disorder: A multimodal brain imaging study," *NeuroImage: Clin.*, vol. 7, pp. 155–169, 2015.
- [45] F. Liem *et al.*, "Predicting brain-age from multimodal imaging data captures cognitive impairment," *NeuroImage*, vol. 148, pp. 179–188, 2017.
- [46] S. Atasoy, I. Donnelly, and J. Pearson, "Human brain networks function in connectome-specific harmonic waves," *Nature Commun.*, vol. 7, Jan. 2016, Art. no. 10340.
- [47] D. S. Bassett, N. F. Wymbs, M. A. Porter, P. J. Mucha, J. M. Carlson, and S. T. Grafton, "Dynamic reconfiguration of human brain networks during learning," *Proc. Nat. Acad. Sci.*, vol. 108, no. 18, pp. 7641–7646, May 2011.
- [48] W. Huang, T. A. W. Bolton, J. D. Medaglia, D. S. Bassett, A. Ribeiro, and D. V. D. Ville, "A graph signal processing perspective on functional brain imaging," *Proc. IEEE*, vol. 106, no. 5, pp. 868–885, May 2018.
- [49] W. Huang, L. Goldsberry, N. F. Wymbs, S. T. Grafton, D. S. Bassett, and A. Ribeiro, "Graph frequency analysis of brain signals," *IEEE J. Sel. Topics Signal Process.*, vol. 10, no. 7, pp. 1189–1203, Oct. 2016.
- [50] J. D. Medaglia *et al.*, "Functional alignment with anatomical networks is associated with cognitive flexibility," *Nature Human Behav.*, vol. 2, no. 2, pp. 156–164, Dec. 2017.
- [51] M. Ménoret, N. Farrugia, B. Padeloup, and V. Gripon, "Evaluating graph signal processing for neuroimaging through classification and dimensionality reduction," in *Proc. IEEE Global Conf. Signal Inf. Process.*, Nov. 2017, pp. 618–622.
- [52] M. G. Preti and D. Van De Ville, "Decoupling of brain function from structure reveals regional behavioral specialization in humans," *Nature Commun.*, vol. 10, no. 1, pp. 1–7, 2019.
- [53] C. Hu, J. Sepulcre, K. A. Johnson, G. E. Fakhri, Y. M. Lu, and Q. Li, "Matched signal detection on graphs: Theory and application to brain imaging data classification," *NeuroImage*, vol. 125, pp. 587–600, Jan. 2016.
- [54] S. Itani and D. Thanou, "Combining anatomical and functional networks for neuropathology identification: A case study on autism spectrum disorder," 2019, *arXiv:1904.11296*.
- [55] A. Brahim, M. H. El Hassani, and N. Farrugia, "Classification of autism spectrum disorder through the graph fourier transform of fMRI temporal signals projected on structural connectome," in *Proc. Int. Conf. Comput. Anal. Images Patterns*, 2019, pp. 45–55.
- [56] S. Mortaheb *et al.*, "A graph signal processing approach to study high density EEG signals in patients with disorders of consciousness," in *Proc. Int. Conf. IEEE Eng. Medicine Biol. Soc.*, 2019, pp. 4549–4553.
- [57] S. I. Dimitriadis, "Multiplexity and graph signal processing of EEG dynamic functional connectivity networks as connectomic biomarkers for schizophrenia patients: A whole brain breakdown," Art. no. 551671, 2019. [Online]. Available: <https://www.biorxiv.org/content/biorxiv/early/2019/08/12/551671.full.pdf>
- [58] T. Proix, A. Spiegler, M. Schirner, S. Rothmeier, P. Ritter, and V. K. Jirsa, "How do parcellation size and short-range connectivity affect dynamics in large-scale brain network models?" *NeuroImage*, vol. 142, pp. 135–149, Nov. 2016.
- [59] O. Esteban *et al.*, "fMRIPrep: A robust preprocessing pipeline for functional MRI," *Nature Methods*, vol. 16, 2019, pp. 111–116.
- [60] R. Goebel, F. Esposito, and E. Formisano, "Analysis of functional image analysis contest (FIAC) data with brainvoyager qx: From single-subject to cortically aligned group general linear model analysis and self-organizing group independent component analysis," *Human Brain Mapping*, vol. 27, no. 5, pp. 392–401, 2006.
- [61] A. Ortega, P. Frossard, J. Kovačević, J. M. Moura, and P. Vandergheynst, "Graph signal processing: Overview, challenges, and applications," *Proc. IEEE*, vol. 106, no. 5, pp. 808–828, May 2018.
- [62] L. Goldsberry, W. Huang, N. F. Wymbs, S. T. Grafton, D. S. Bassett, and A. Ribeiro, "Brain signal analytics from graph signal processing perspective," in *Proc. IEEE Int. Conf. Acoust., Speech Signal Process.*, 2017, pp. 851–855.
- [63] J. D. Gibbons and S. Chakraborti, *Nonparametric Statistical Inference*. Berlin, Germany: Springer, 2011.
- [64] C. Fritz, P. Morris, and J. Richler, "Effect size estimates: current use, calculations, and interpretation," *J. Exp. Psychol.: General*, vol. 141, no. 1, pp. 2–18, 2012.
- [65] R. Zafar, A. S. Malik, N. Kamel, and S. C. Dass, "Role of voxel selection and roi in fMRI data analysis," in *Proc. IEEE Int. Symp. Med. Meas. Appl.*, 2016, pp. 1–6.
- [66] R. A. Poldrack, "Region of interest analysis for fMRI," *Social Cogn. Affect. Neurosci.*, vol. 2, no. 1, pp. 67–70 1749–5016, 2007.
- [67] E. Vul and N. Kanwisher, "Begging the question: The non-independence error in fMRI data analysis," in *Foundational Issues Human Brain Mapping*, 2010, pp. 71–91.
- [68] T. Caliński and J. Harabasz, "A dendrite method for cluster analysis," *Commun. Statist.-Theory Methods*, vol. 3, no. 1, pp. 1–27, Jan. 1974.
- [69] P. J. Rousseeuw, "Silhouettes: A graphical aid to the interpretation and validation of cluster analysis," *J. Comput. Appl. Math.*, vol. 20, pp. 53–65, 1987.
- [70] J. M. Silver, T. W. McAllister, and D. B. Arciniegas, "Depression and cognitive complaints following mild traumatic brain injury," *Amer. J. Psychiatry*, vol. 166, no. 6, pp. 653–661, 2009.
- [71] E. D. Bigler, "Anterior and middle cranial fossa in traumatic brain injury: Relevant neuroanatomy and neuropathology in the study of neuropsychological outcome," *Neuropsychology*, vol. 21, no. 5, pp. 515–531, 2007.
- [72] E. B. McClure-Tone *et al.*, "Preliminary findings: Neural responses to feedback regarding betrayal and cooperation in adolescent anxiety disorders," *Developmental Neuropsychology*, vol. 36, no. 4, pp. 453–472, 2011.
- [73] C. P. Furtado, J. J. Maller, and P. B. Fitzgerald, "A magnetic resonance imaging study of the entorhinal cortex in treatment-resistant depression," *Psychiatry Res.: Neuroimag.*, vol. 163, no. 2, pp. 133–142, 2008.
- [74] K. B. Koh, J. I. Kang, J. D. Lee, and Y.-J. Lee, "Shared neural activity in panic disorder and undifferentiated somatoform disorder compared with healthy controls," *J. Clin. Psychiatry*, vol. 71, no. 12, pp. 1576–1581, 2010.
- [75] T. B. Meier, M. A. Lancaster, A. R. Mayer, T. K. Teague, and J. Savitz, "Abnormalities in functional connectivity in collegiate football athletes with and without a concussion history: Implications and role of neuroactive kynurenine pathway metabolites," *J. Neurotrauma*, vol. 34, no. 4, pp. 824–837, 2017.
- [76] C. A. Orr *et al.*, "Neuroimaging biomarkers of a history of concussion observed in asymptomatic young athletes," *J. Neurotrauma*, vol. 33, no. 9, pp. 803–810, 2015.
- [77] D. J. Sharp *et al.*, "Default mode network functional and structural connectivity after traumatic brain injury," *Brain*, vol. 134, no. 8, pp. 2233–2247, Aug. 2011.
- [78] Y. Zhou *et al.*, "Mild traumatic brain injury: Longitudinal regional brain volume changes," *Radiology*, vol. 267, no. 3, pp. 880–890, 2013.
- [79] M. L. Keightley *et al.*, "A functional magnetic resonance imaging study of working memory in youth after sports-related concussion: Is it still working?" *J. Neurotrauma*, vol. 31, no. 5, pp. 437–451, 2013.
- [80] J. A. Wolf and P. F. Koch, "Disruption of network synchrony and cognitive dysfunction after traumatic brain injury," *Frontiers Syst. Neurosci.*, vol. 10, p. 43, 2016.
- [81] A. Tarazi *et al.*, "Motor function in former professional football players with history of multiple concussions," *J. Neurotrauma*, vol. 35, no. 8, pp. 1003–1007, 2018.
- [82] K. Misquitta *et al.*, "The relationship between brain atrophy and cognitive-behavioural symptoms in retired canadian football players with multiple concussions," *NeuroImage: Clin.*, vol. 19, pp. 551–558, 2018.
- [83] T. D. Stein, V. E. Alvarez, and A. C. McKee, "Concussion in chronic traumatic encephalopathy," *Current Pain Headache Rep.*, vol. 19, no. 10, p. 47, Aug. 2015.
- [84] E. L. Breedlove *et al.*, "Biomechanical correlates of symptomatic and asymptomatic neurophysiological impairment in high school football," *J. Biomechanics*, vol. 45, no. 7, pp. 1265–1272, 2012.
- [85] A. C. McKee *et al.*, "Chronic traumatic encephalopathy in athletes: Progressive tauopathy after repetitive head injury," *J. Neuropathol. Exp. Neurol.*, vol. 68, no. 7, pp. 709–735, 2009.
- [86] A. C. McKee *et al.*, "TPD-43 proteinopathy and motor neuron disease in chronic traumatic encephalopathy," *J. Neuropathol. Exp. Neurol.*, vol. 69, no. 9, pp. 918–929, 2010.
- [87] Y. Benjamini and Y. Hochberg, "Controlling the false discovery rate: A practical and powerful approach to multiple testing," *J. Roy. Statistical Soc.: Ser. B (Methodological)*, vol. 57, no. 1, pp. 289–300, Jan. 1995.